

A Search for Spectral Galaxy Pairs of Overlapping Galaxies based on Fuzzy Recognition

Haifeng Yang^{1,2,3}, Ali Luo^{1*}, Xiaoyan Chen¹, Jifu Zhang², Wen Hou³, Jianghui Cai², Peng Wei³, Juanjuan Ren³, Xiaojie Liu³, Yongheng Zhao¹

¹Key Laboratory of Optical Astronomy, National Astronomical Observatories, Chinese Academy of Sciences, Beijing 100012, China

²School of Computer Science and Technology, Taiyuan University of Science and Technology, Taiyuan, 030024, China

³University of Chinese Academy of Sciences, Beijing 100049, China

23 March 2022

ABSTRACT

The Spectral Galaxy Pairs (SGPs) are defined as the composite galaxy spectra which contain two independent redshift systems. These spectra are useful for studying dust properties of the foreground galaxies. In this paper, a total of 165 spectra of SGPs are mined out from Sloan Digital Sky Survey (SDSS) Data Release 9 (DR9) using the concept of membership degree from the fuzzy set theory particularly defined to be suitable for fuzzily identifying emission lines. The spectra and images of this sample are classified according to the membership degree and their image features, respectively. Many of these 2nd redshift systems are too small or too dim to select from the SDSS images alone, making the sample a potentially unique source of information on dust effects in low-luminosity or low-surface-brightness galaxies that are under-represented in morphological pair samples. The dust extinction of the objects with high membership degree is also estimated by Balmer decrement. Additionally, analyses for a series of spectroscopic observations of one SGP from 165 systems indicate that a newly star-forming region of our Milky Way might occur.

Key words: methods: data analysis-galaxies:ISM-dust:extinction-galaxies: evolution-galaxies: emission lines

1 INTRODUCTION

The evolutionary track of a galaxy can be shaped as its merger history, which largely depends on the properties of the rich environments. Since one of the first observations (Dressler & Alan 1980) showed that the environment may influence the properties of galaxies, numerous further identification studies have been carried out. The environmental impacts on galaxies in clusters (especially in over-dense clusters) (Wake et al. 2005; Tyler et al. 2013), galaxy groups (Wilman et al. 2008; Hou et al. 2013), or galaxy pairs (Krabbe et al. 2014) have always been hot issues for observations and researches. Furthermore, it has been accepted that the density on smaller scales can be the major impetus behind the galaxy evolution (Lewis et al. 2002; Blanton & Berlind 2007), and galaxy mergers may provide the most obvious mechanism. Thus, astronomers have paid a lot of attentions on galaxy pairs. From different perspectives, in-

teracting effects of galaxy pairs were extensively analyzed in a series of works (Ellison et al. 2008, 2010; Patton et al. 2011; Ellison et al. 2011; Scudder et al. 2012; Patton et al. 2013; Ellison et al. 2013a,b), which are the most influential works in this decade. They found that there was an enhancement in the star formation rate (SFR) of galaxy pairs. And the intensity of this enhancement is mainly correlated to galaxy evolutionary phases (the enhancement in late-type galaxies is more significant than that in early-type ones, see Nikolic et al. 2004), stellar masses relationship (major pairs are higher than others) and their separations (this enhancement increases as pair separation decreases). The latest research (Satyapal et al. 2014) also showed that the fraction of AGN in the pairs increases with decreasing projected separation. In general, one criteria to differentiate the interacting and non-interacting galaxy pairs is the distance (or velocity difference Δv or redshift difference Δz) between the two galaxies.

Further, overlapping galaxy pairs on the line of sight are very valuable materials for dust studies. Dust composes only a small fraction of the interstellar medium in galaxies,

* Email: lal@nao.cas.cn

but plays an important role in understanding the fundamental cosmological parameters. These parameters are useful for determining the mass density and the cosmological constant, as well as understanding the measured star-formation rates of the higher redshift proto-galaxies in the early universe. Dust extinction and dust mass can be estimated from differential photometry in occulting pairs of galaxies, which was firstly proposed by [White & Keel \(1992\)](#), and then applied to the known pairs by using ground-based optical images ([Domingue et al. 1999](#)), spectroscopy ([Domingue et al. 2000](#)) and later space-based HST images ([Keel & White III 2001](#); [Holwerda & Keel 2013](#)). The flux ratio of two Balmer emission lines from nebular (such as $H\alpha/H\beta$) can be used to determine the dust extinction as well ([Kennicutt & Robert 1992](#)). Recently, more pairs were found in the SDSS spectroscopic catalogue (86 pairs, see [Holwerda et al. 2007a](#)) and in the Galaxy Zoo project (1993 pairs, see [Keel et al. 2013](#)). The sample selection is mainly based on photometric images. It is difficult and time-consuming to search these targets in images automatically, especially for some superimposed galaxies ([Domingue et al. 2000](#)). Currently, there are few auto-search methods for dual-redshift system in spectra. Cross-correlation analysis results have been reported from SDSS DR7, which can provide several redshifts candidates for every spectrum, and finally increased the data dimensions. Thus, it is more suitable for verifying multi-redshift systems. [Tsalmantza & Hogg \(2012\)](#) have proposed a mathematical approach to fitting the spectral models at different redshifts, simultaneously. This method depends on both the training model and optimization strategy. Fortunately, the emission-line galaxy pairs in nearby universe may also be distinguished by aid of composite spectra, i.e. SGP.

In this paper, a novel SGP search method based on fuzzy recognition is presented and especially focused on searching for ‘emission+emission’ dual-redshift system spectra from the SDSS DR9. As a result, a total of 165 spectra of SGPs are provided, and the spectra and images of this sample are classified according to the membership degree and their image features, respectively. For the objects with high membership degree, the dust extinction is also estimated by Balmer decrement. Additionally, analyses for a series of observations of one SGP from 165 systems indicate that a newly star-forming region of our Milky Way might occur.

The paper is organized as follows. In Section 2, sample selection and auto-search method are described in detail. A SGP list, results analysis and preliminary discussion of extinction estimation are shown in section 3. Finally, a summary of the main work is given in section 4.

2 AUTOMATED SEARCH METHOD

2.1 Sample selection

The ninth data release of the Sloan Digital Sky Survey (SDSS DR9, see [Ahn et al. 2012](#)) is the first release of the spectra from the SDSS-III’s Baryon Oscillation Spectroscopic Survey (BOSS), in which about 1.5 million (1, 457, 002) massive galaxies’ spectra were presented. We are honoured to get these data and choose them as the initial data set of this work. To obtain the final sample, we reduce these spectra firstly according to the following criteria.

All spectra of galaxy from SDSS DR9 are selected as our initial data set. Here, we do not impose the subclass limit on the spectra selection although our searching is especially focused on the galaxy spectra with two groups of emission lines, and it is mainly to avoid missing the SGPs of other subclasses automatically classified by pipeline. For example, the object NO.100 in Table 1 is a SGP, while its subclass provided by the SDSS is ‘null’. Thus, as long as two sets of emission lines appear in a spectrum, the spectrum is kept as a candidate.

In order to guarantee that both $H\alpha$ and $H\beta$ fall simultaneously in the SDSS spectral wavelength coverage, we limit redshift range to $z \leq 0.4$. Thus, some other emission lines such as $O\ II\ \lambda\lambda 3727, 3730$, $O\ III\ \lambda\lambda 4960, 5008$, $N\ II\ \lambda\lambda 6550, 6585$ could also be employed in auto-search process.

Furthermore, it is the fitting quality of the emission lines (instead of the SNR) that is used to define the membership degree, which is utilized in searching process to measure the confidence of a spectrum belonging to SGPs (see section 2.2.1).

2.2 Method description

There are many uncertain or imprecise characteristics increasing the difficulty of auto-identification. For example, not all positive signal (e.g. noise) is true emission line; not all the emission lines have peak value for various reasons such as sky subtraction error; and some emission lines are weakened by stellar absorption, such as $H\beta$. As mentioned above, the spectral shapes of these objects vary a lot due to their different observation environments, broadening, redshifts, and processing errors. Therefore, it is desirable to find a method which can process and analyze the uncertain data.

In mathematics, fuzzy sets ([Zadeh 1965](#)) are sets whose elements have degrees of membership, and now used in different areas, such as linguistics, decision-making and clustering ([Zhang et al. 2014, 2013](#)). By contrast with the classical set theory, fuzzy set theory described with the aid of a membership function valued in the real unit interval $[0, 1]$ permits the gradual assessment of the membership of elements in a set. In our method, this idea of the gradual assessment is introduced into the line identification.

In brief, identifying emission lines in a spectrum through fuzzy recognition is the first key step of our method. And then the emission lines with the redshift are subtracted from the spectrum. Finally, the first step is repeated twice in the residual spectrum.

2.2.1 Fuzzy recognition and membership degree

Let pair (O, m) be a fuzzy set of SGPs where O is a galaxy spectra set and m is a mapping function ($O \rightarrow [0, 1]$). For each spectrum $x \in O$, the value $m(x)$ is called the membership degree of x in (O, m) . In other words, every element x in O has a degree $m(x)$ belonging to SGPs. Meanwhile, the membership degree of every spectrum can be defined by the quality and related characteristics of some spectral lines. Here, we choose emission lines $\{H\alpha\ \lambda 6565, H\beta\ \lambda 4862, O\ III\ \lambda\lambda 4960, 5008, N\ II\ \lambda\lambda 6550, 6585, S\ II\ \lambda\lambda 6718, 6733\}$ as L , and define the parameter d by equation (1) for every emission

line of each spectrum. Thus the $m(x)$ is an average of all d in L .

$$d(\text{factor}, \text{fit}_{err}, \text{peak}) = (k_1 * \text{factor}) + (k_2 * \text{fit}_{err}) + (k_3 * \text{peak}) \quad (1)$$

where k_1, k_2, k_3 are the proportions (weights) of the three parameters respectively and $\text{sum}(k_1, k_2, k_3) = 1$.

The parameter factor: The parameter *factor* is defined as equation (2):

$$f(x, y) = \begin{cases} 0, & R_x \cap R_y + \Delta\lambda_{xy} = \Phi \text{ or} \\ & \text{coreErr}_x \geq 99 \\ 1, & \text{core}_x \in R_y + \Delta\lambda_{xy} \\ \frac{R_y[-1] + \Delta\lambda_{xy} - R_x[0]}{\text{coreErr}_x}, & \text{core}_x \geq R_y[-1] + \Delta\lambda_{xy} \\ \frac{R_x[-1] - R_y[0] - \Delta\lambda_{xy}}{\text{coreErr}_x}, & \text{core}_x \leq R_y[0] + \Delta\lambda_{xy} \end{cases} \quad (2)$$

where $x, y \in L$, core and core_{err} is the line center and the corresponding error respectively when fitted by Gaussian function, $R = [\text{core} - \text{core}_{err}, \text{core} + \text{core}_{err}]$ is acceptable range of the core, $R[0]$ is the left border, $R[-1]$ is the right one, and $\Delta\lambda$ is the difference of two lines' rest wavelength provided by SDSS.

Assuming that y is a known line with the best fitting quality by Gaussian function, we can use $f(x, y)$ as the main parameter to measure the confidence of x belonging to the set L . We suppose that $\Delta\lambda_{xy} = (\text{wavelength}_y - \text{wavelength}_x)_{rest} * (1+z)$, $H\alpha$ is a known line with best fit quality, $R\alpha$ is the core range of $H\alpha$, and $H\beta$ is a line to identify. Then $R\alpha + \Delta\lambda_{\alpha\beta}$ is the theoretically acceptable wavelength range of $H\beta$. So it is certainly accepted as $H\beta$ when $\text{core}_\beta \in R\alpha + \Delta\lambda_{\alpha\beta}$, rejected when $R\beta \cap R\alpha + \Delta\lambda_{\alpha\beta} = \Phi$, and otherwise, accepted as a certain degree estimated by equation (2), whose value is inversely proportional to the deviation of core_β from $R\alpha + \Delta\lambda_{\alpha\beta}$ and is in a real unit interval $[0, 1]$.

The parameters fit_{err} : In addition, the whole fitting error fit_{err} also needs concern. The smaller the fit_{err} is, the stronger confidence the line has. And when $\text{fit}_{err} \geq 99$ (99 is the default number when fitting $\chi^2 \geq 99$), the line should not be accepted. Then the function $\text{fit}_{err}(x)$ is,

$$\text{fit}_{err}(x) = \begin{cases} 0, & \text{Err}_{all} \geq 99 \\ 1, & \text{Err}_{all} \leq 1 \\ (99.0 - \text{Err}_{all}) / \text{Err}_{all}, & \text{others} \end{cases} \quad (3)$$

where $x \in L$ and Err_{all} is the sum of fitting errors by Gaussian function.

The parameter peak: Similarly, stronger emission lines are more favoured in searching. Therefore after normalizing the flux by the standard deviation, a function *peak*(x) is defined as

$$\text{peak}(x) = \begin{cases} 1, & \text{peak}_{flux} \geq 10 \\ \text{peak}_{flux} / 10, & \text{others} \end{cases} \quad (4)$$

2.2.2 A Spectral Galaxy Pairs search algorithm

The algorithm is described as follows:

(i) select 1D Galaxy Spectra Set A as the initial data set, and $N1, N2, m1, m2$ as input parameters ($N1$ and $N2$ are

Table 1. Pre-searching rules

Integrated flux	Peak flux
$H\alpha_I \geq H\beta_I$	$H\alpha_P \geq H\beta_P$
$N_{II} \lambda 6550_I \leq N_{II} \lambda 6585_I$	$N_{II} \lambda 6550_P \leq N_{II} \lambda 6585_P$

thresholds of lines number ($\leq |L|$). $m1$ and $m2$ are thresholds of lines membership degree.)

(ii) select a spectrum of A, traverse each emission signal in the wavelength region ($\geq 6000\text{\AA}$)

(iii) choose the strongest one as $H\alpha$ emission line candidate, and if there is no emission signal in this wavelength region turn to next spectrum (*The flag of emission signal is average* ($\text{flux}_{[\text{linecore}-3, \text{core}+3]} \geq \text{average}(\text{flux}_{[\text{linecore}-5, \text{core}+5]})$))

(iv) calculate the temporary redshift $z1$ by $H\alpha$ line, then calculate the wavelength of other lines in L according to $z1$, and calculate the peak flux as well as integral flux in region $\pm 5\text{\AA}$ for each line

(v) set emission lines initial number $N = 0$

(vi) check wavelength positions of these lines. If there is an emission line on current position, do the following two steps:

a: let $N=N+1$,

b: fit this emission line by Gaussian function and quadratic polynomial, and calculate the parameter $d_{\text{currentLine}}$

(vii) check the following conditions in Table 2

(*Average* (d in L) $\geq m1$, $N \geq N1$, *Table 1 conditions and* $z1 \leq 0.4$), if True, turn to step (viii), otherwise mask current $H\alpha$ line and turn to step (iii)

(viii) subtract these emission lines ($H\alpha$ and other lines of current redshift system)

(ix) search the next redshift system by using the same method as step (iii–viii) (*The check conditions in step (vii) change to Average* (d in L) $\geq m2$, $N \geq N2$, $0 \leq z2 \leq 0.4$, and $z2 - z1 \geq 0.005$)

If success, add this spectra into SGP candidate set B and turn to step (x); Otherwise, go to step (x) directly

(x) select next spectrum, loops steps (ii–x) until all spectra in A have been examined

(xi) record Candidate Set B

We also compare both redshifts calculated by our method with the one provided by SDSS pipeline and find that the results have a good agreement. Besides, all the spectra in the candidate set B are further checked by eyes or various searching rules, which is discussed in the next section.

2.2.3 Searching rules and results

This algorithm can be briefly divided into two steps: reduced by the pre-searching rules and identified by fuzzy recognition.

Pre-searching rules. The data set is firstly reduced according to the pre-searching rules listed in Table 1. These rules are defined to remove those spectra that are absolutely not SGP from the data set avoiding unnecessary line fittings. As seen in the Table 1, the integrated flux and peak flux values of the emission lines are both used so that the

Table 2. Results in different thresholds

Table 1 ^a	Conditions			Record Count	
	m1 ^b	m2 ^c	N ^d	auto ^e	identify ^f
✓	≥0.60	≥0.70	≥3	504	44
✓	≥0.40	≥0.60	≥3	858	108
✓	≥0.30	≥0.40	≥3	6004	142
✓	≥0	≥0	≥3	55092	165

^a The ‘✓’ indicates that the sample is firstly reduced according to the criteria listed in Table 1.

^b The ‘m1’ is membership degree threshold and in ‘m1’ calculation process each element degree of L is calculated by equation 1 with input parameters: { $k_1 : 0.4, k_2 : 0.1, k_3 : 0.5$ }. Values in this table are the empirical thresholds.

^c The ‘m2’ is membership degree threshold and in ‘m2’ calculation process each element degree is calculated by equation 1 with input parameters: { $k_1 : 1, k_2 : 0, k_3 : 0$ }. Values in this table are the empirical thresholds.

^d The ‘N’ is the sum of emission signal of a spectrum detected in searching process. In the experiment, N1 and N2 is set the same low threshold N. Values in this table are the empirical thresholds.

^e The record count of auto searched.

^f The record count of spectra identified visually.

misjudgements caused by noises or sky subtraction errors are controlled as small as possible. It should be noted that high order Balmer lines (very weak in some spectra) and some strong oxygen lines (such as O II $\lambda\lambda 3927, 3930, \text{O III } \lambda\lambda 4960, 5008$ with no certain relationship between the strength of these lines) are not chosen as reduced criteria. After two checks for every spectrum in the data set, 55092 spectra remain.

Membership degree thresholds. The membership degree can fuzzily measure the confidence of a spectra belonging to the SGPs. Therefore, a reasonable choice of membership degree thresholds is vitally important in the recognition process. We have tried several groups of membership degree thresholds from loose to strict and visually checked every candidate mined out by the method mentioned above. Table 2 shows the corresponding results of different thresholds. As seen from this table, along with the search conditions becoming looser from line 1 to line 4, the record count of SGPs gets larger and the confidence of these spectra in SGPs gets lower simultaneously. It is believed that the quality of new members admitted into SGPs is very poor if the conditions get much looser.

The limitation of redshifts difference. To test the ability of this approach on the redshifts difference limitation, some experiments are implemented. A test sample of 113 star-forming galaxies spectra with SNR ≥ 50 is chosen from DR9 data. Then, any two spectra, which are transformed to rest wavelength and normalized, are combined according to the mode: the redshift $z_1 = 0, z_2$ are random numbers generated from different intervals (column 1 of Table 3), and $flux = flux_a + k * flux_b$ where $k \in [0.5, 1.5]$. Thus, five groups of synthetic spectra with dual-redshift system are produced and applied in test. As seen from the results, almost all spectra can be recognized when $\Delta z \geq 0.005$, although few objects missed since the signal is too weak. The missed spectra can also be recognized when $k = 1.5$. How-

Table 3. Δz limit test results

The range of Δz	Spectra count	Recognized success	
		$k \in [0.5, 1.5]$	$k=1.5$
0 ~ 0.001	27	0	0
0.001 ~ 0.003	29	2	2
0.003 ~ 0.005	23	5	9
0.005 ~ 0.008	23	21	23
0.008 ~ 0.015	47	43	47

ever, the search method for SGPs (physically interacting pairs) of $\Delta z \leq 0.005$ still need to be further explored in follow-up works. In a word, the lower limit of Δz in the searching process is set to 0.005.

3 RESULTS AND ANALYSIS

3.1 SGPs sample selected from SDSS DR9

Table 1 in Appendix lists the SGPs sample searched from SDSS DR9 by the method mentioned above. This sample includes 165 spectra which have two redshift systems. Each spectrum is assigned a serial number (shown in column 1) that will be referred to throughout this paper. The basic information of these objects (including SDSS ID, RA, DEC) are gathered from the Catalogue Archive Server Jobs System of SDSS DR9 and listed in this table from column 2 to column 4.

Two redshifts (column 5, 6) are estimated by using the observed central wavelength and the rest central wavelength of the lines in the searching process. The corresponding errors are derived from the fitting errors of the line cores. These redshifts are also crossed with XCRedshift results of SDSS DR7 (The same values of DR9 or later release are not found). The serial numbers are marked with asterisks in the upper right corner if there are at least two values in XCRedshift results close to the values given by the proposed method in this paper.

The confidence of spectra belonging to SGPs may vary due to different thresholds. Some spectra show very obvious characteristics in both systems, while others do not. For the latter, the lines coming from the background galaxies, can hardly be identified. In this view, these objects are divided into four grades according to different threshold values. The spectra met the conditions of line 1 in Table 2 are graded as ‘A’, line 2 as ‘B’, line 3 as ‘C’, and line 4 as ‘D’, respectively (column 7 in Table 1). Figure 1 shows four examples with different grades. It is noted that the grade only reflects the average fitting quality of the emission lines. And some of the weak lines may lead to the lower grade of the spectrum. Therefore some of the low-level spectra may be not reliable and require further identification.

Some objects of the sample have been observed several times. For example, the object ‘SDSS J131105.31+022528.3’ has two spectra: No.29 and No.30, both of which appear two redshift systems. Here, for the similar objects, we only kept one spectrum with the most obvious dual-redshift system to avoid redundancy. The object ‘SDSS J030848.14+004659.9’ (No.74), with several spectra from different observations, is a special case. It will be separately discussed later. Additionally, the basic information of No. 130 has not been found.

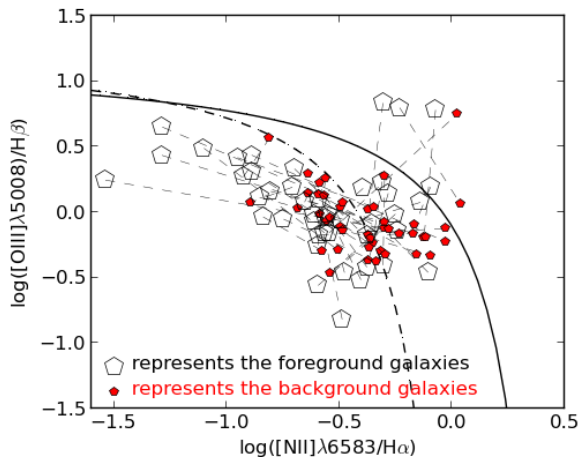


Figure 2. The emission-line ratio diagnostic diagram (i.e. BPT diagram) for 44 sources of Grade ‘A’. The solid curve defined by Kewley et al. (2001) and dashed curve defined by Kauffmann et al. (2003) show the separation among star-forming galaxies, composite galaxies and AGNs. Two members of one spectrum are connected by a dashed line.

Its Object Name is replaced by the key values string ‘Plate-MJD-Fiber’, the RA and DEC are valued ‘None’ in Table 1.

3.2 Spectra and image analysis

Our sample is searched based on spectra rather than the images, since those galaxies which are difficult to detect in the images can also be traced via constraints on redshifts from spectra. Figure 1 & 3 show some examples, both redshift systems of which are marked with dashed lines of different color. In these spectra, the most notable features are the strong emissions of H α band, O III λ 5008 band and O II $\lambda\lambda$ 3727, 3729. The emission lines of most foreground galaxies are stronger than that of the background ones, and only a few spectra show the contrary appearance.

For most spectra in this sample, the first (low) redshift systems always show obvious and strong features in the emission lines, while the second (high) redshift systems are relatively weak. Only a few SGPs show an opposite situation, which may be interesting since the foreground galaxy may be lost in the background light in the images. It is hard to clearly explain every scenes under current conditions since many factors may increase its complexity, such as dust density of foreground galaxy (opacity), varied redshifts, interstellar medium (ISM) features and different parts of the galaxy the fibre traced. Decomposition of the two members in spectra is also difficult because the luminosity contributions of the two members are not easy to determine accurately. Improving a mathematical approach, such as stellar population synthesis code ‘STARLIGHT’ (Chen et al. 2009), may be a good choice. Figure 2 shows the two members’ locations of those objects graded ‘A’ in BPT (Kauffmann et al. 2003) diagram. The locations between the two members have no correlation in this diagram since that two different components without interactions may appear in one spectrum only because of superimposition in the line of sight. Most of the pairs are located in the H II region or composite region.

3.2.1 Some special cases

For the redshift difference of galaxies pairs, 0.008 is a very conservative value which would distinguish (non-)associated galaxies (Keel et al. 2013). From this viewpoint, most of the SGPs in this sample are non-interacting galaxy pairs. The maximum Δz is 0.27 and the light from the background galaxy of this pair is very faint. On the contrary, the minimum value $\Delta z \sim 0.0055$ (see the top panel in Figure 3) indicates that the two members may have weak interactions. As seen in this spectrum, the emission line N II λ 6585 of the foreground galaxy and N II λ 6550 of the background one are superimposed, which leads to a change of the line profile. That is why most close pairs are missed in the searching.

No.84 (see the second panel in Figure 3) is also an interesting case. The background galaxy appears to be an extremely metal-poor galaxy. And it is located on the end of left wing of the SEAGal (Kewley et al. 2001) in the BPT diagram, which suggests that the target is still in H II regions. In the H α band, N II double lines and S II double lines are almost invisible. The O II $\lambda\lambda$ 3727, 3730 are also very weak. However, the O III λ 5007 is surprisingly strong. This feature is in stark contrast to the foreground galaxy, in which the O II double lines is stronger than O III λ 5007. We speculate that it was not caused by the dust extinction effects of its foreground partner since the Balmer decrement values (H α /H β) of the two objects are very close. The way how this spectrum forms needs further exploring.

No.83 (see the third panel in Figure 3) may have three redshift systems although the confidence is very low. The triplet-redshift spectra are very rare since they requires not only more than three galaxies in the line of sight, but also the emission lines triggering from overlapping areas traced by the same fibre. Even for the dual-redshift galaxy spectra, the sample (including some sources may be not true SGPs) provided in this paper is very small and occupies only 0.01 % of the total galaxies spectra. In the spectrum of No.83, the first redshift system has obvious features, while the second and the third redshift system is not reliable. Especially in the third system, S II double lines are somewhat unusual, H β , O II lines do not appear in this spectrum, and O III λ 4364 line is covered by the O III λ 5007 line of the first system. Therefore, we speculate that the identification of H α band lines in the third system may be interfered by noise.

In this sample, there are 18 spectra (such as No.22, 23, 24, and so on) with one redshift close to 0. The bottom panel of Figure 3 is an example (No.23). These objects are all located in sky area of Galactic anti-center ($135^\circ < l < 225^\circ$, $-45^\circ < b < 45^\circ$). In this direction, light from the star forming regions of the Galactic arms or local galaxies clusters (such as M31) may have more chances to sneak into fibres. Therefore, the 0-redshift systems (the redshift is very close to zero) may appear in these spectra. These spectra are useful to study the structure and evolution of our Milky Way. Among these objects, No.74 is very special. This object has been carried out nine spectroscopic observations (shown in Figure 4) by SDSS, and dual-redshift system appears only in the spectrum of the latest observation. In its 0-redshift system, H α band has obvious emission lines while other lines are almost invisible. Moreover, the H α and N II λ 6585 lines just coincide with the O I lines of the background galaxy. It may result in wrong recognition by pipeline. The series

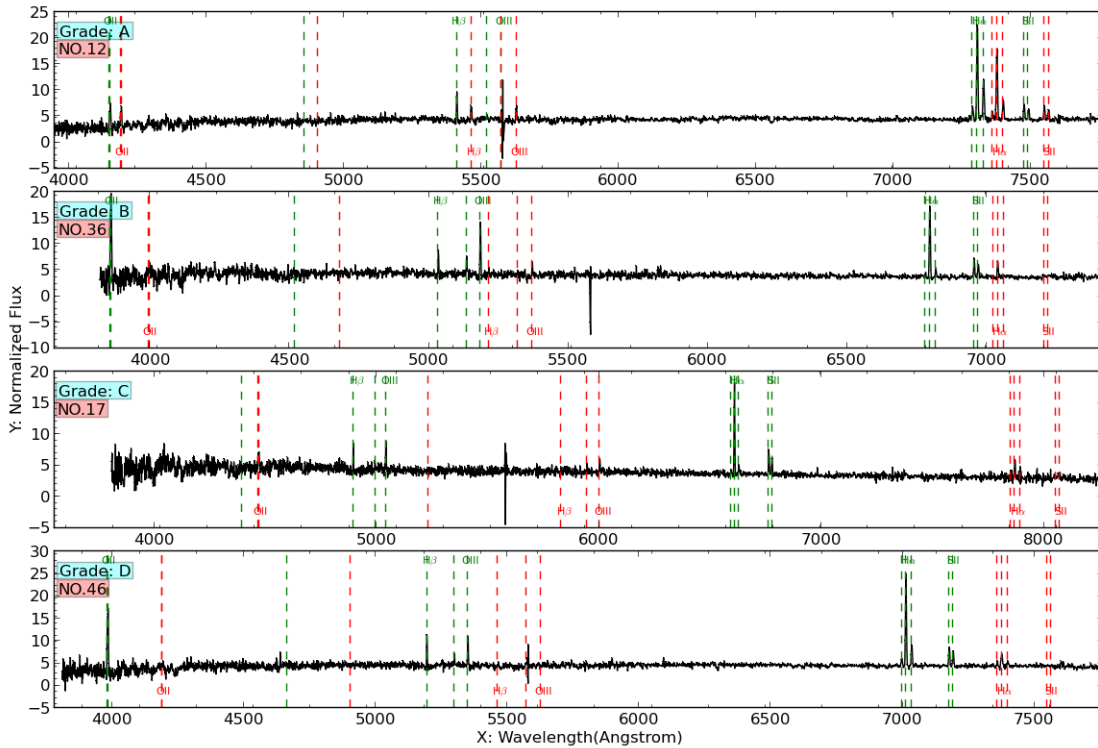


Figure 1. Four examples randomly selected from each grade level (A, B, C, D) spectra. The grade level and the serial number are labelled on the top left corner of each spectrum. Two groups of common emission lines in optical band, including $\{O\text{ II } \lambda\lambda 3727, 3730, H\beta, O\text{ III } \lambda\lambda 4960, 5008, H\alpha, N\text{ II } \lambda\lambda 6550, 6585, S\text{ II } \lambda\lambda 6718, 6733\}$, are marked with red and green dashed lines, respectively.

of spectra in Figure 4 indicate that the star-forming region occurs in recent years.

3.2.2 The image analysis

In fact, the SGPs are different from the galaxy pairs. Galaxy pairs generally mean the binary systems with only two close objects. However, a SGP implies such a scene that one component exists behind its foreground partner and the emission lines are triggered in their overlapped parts. In other words, they may exist in the environment of galaxy pairs, galaxy groups, galaxy clusters, or even super galaxy clusters. To understand the scenes of their environment, photometric image is also necessary. So all images of this sample provided by SDSS are checked visually and divided into two basic classes, eight subclasses (see column 8 in Table 1) according to projection features and related literature (see column 9 in Table 1). The classification criteria of the basic class is whether the objects in one image can be distinguished (Figure 5) or not (Figure 6). The details are as follows:

FPV (Face-on-Pair-Visible): Two galaxies can be separated visually in the image and they are all faced on to us. The upper two rows of Figure 5 are four examples. For the first two sources, the visual sizes of the pairs are close in the images while that of the other two sources differ considerably. The target may be a satellite galaxy of another large galaxy.

FGV (Face-on-Group-Visible): They are multiple galaxy systems. Most of the galaxies in these systems are faced on to us and several objects can be separated in the

images. It is noted that all sources appearing in the galaxy group, galaxy cluster or other large size structure samples in literature (see column 9 in Table 1) are classified as ‘Group’. So there may be some sources showing only two galaxies in their images. The third and fourth row of Figure 5 are four examples.

EPV (Edge-on-Pair-Visible): The main difference with FPV is that these galaxies are edge-on to us. The fifth and sixth row of Figure 5 also show four examples.

EGV (Edge-on-Group-Visible): The main difference with FGV is that these galaxies are edge-on to us. Unfortunately, it is very difficult to distinguish from the images. So no source in our list is classified as EGV.

Figure 6 shows another four subclasses examples which can not be easily separated from the images. In other words, the background galaxies are highly overlapped with the foreground ones. The main basis of this classification is from the related literature. Similar to the previous four subclasses mentioned above, they are **FPI (Face-on-Pair-Invisible)**, **FGI (Face-on-Group-Invisible)**, **EPI (Edge-on-Pair-Invisible)** and **EGI (Edge-on-Group-Invisible)**, respectively.

3.3 Dust extinction measurement

The effective dust extinction value can be measured successfully from pairs of overlapping galaxies in the nearby universe. This geometry of SGPs enables us to directly measure the extinction of light from the background galaxy as it passes through the foreground galaxy. The Balmer decre-

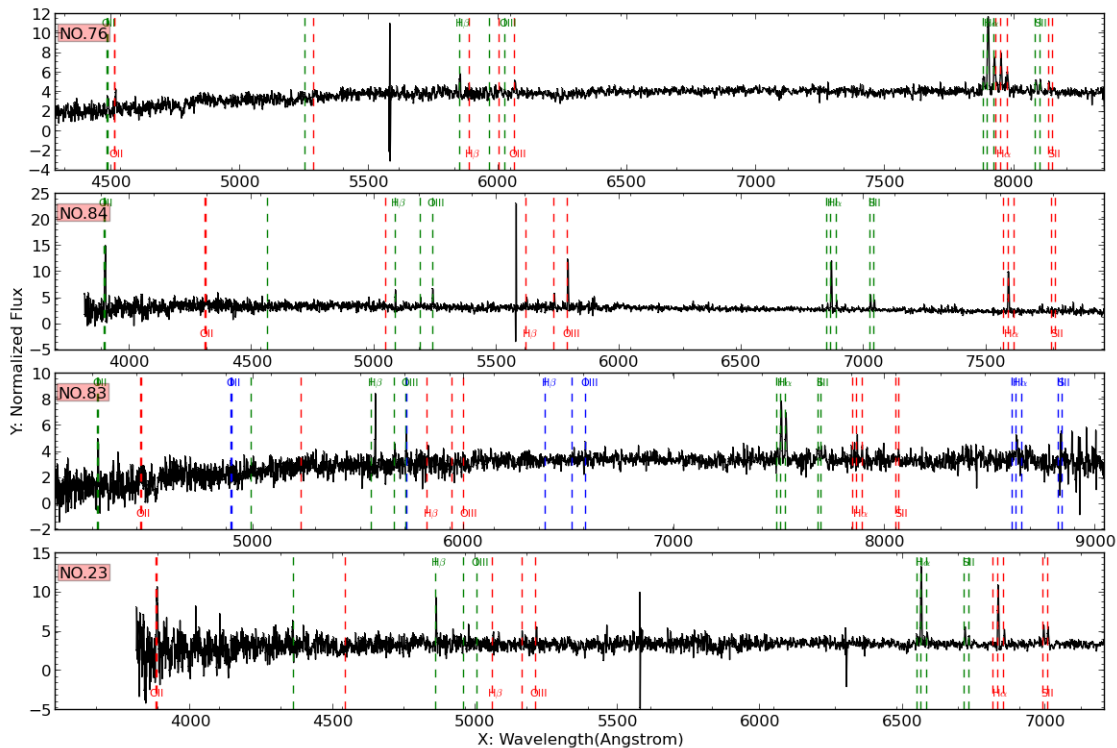


Figure 3. Four special spectra: the first panel spectrum indicates that the two objects may be interacting pairs. The second panel is an interesting spectrum with strange oxygen lines. The third spectrum may have three redshift systems and emission lines of the third redshift are marked with blue dashed lines. And the last one is an example whose foreground emission are from the Milky Way. All symbols are the same as Figure 1.

ment can also be used to determine the extinction. The values of $H\alpha/H\beta > 2.86$ (Calzetti et al. 2000) show extinction under the conditions normally assumed for galaxy H II regions. Due to the dependence on the measurement accuracy of emission lines, the $H\alpha/H\beta$ values for only the two members of those targets graded ‘A’ are reported in Table 4. And the $H\alpha/H\beta$ values are used to derive the extinction values according to equation 5 described below:

$$E(B - V)_{H\alpha/H\beta} = \frac{2.5}{k(H\beta) - k(H\alpha)} \log\left(\frac{H\alpha/H\beta}{2.86}\right) \quad (5)$$

where $k(H\alpha)$ and $k(H\beta)$ are taken from Calzetti et al. (2000). The results are also listed in Table 4.

Some extinction values may be higher than the values derived from photometric magnitude. We infer that it is reasonable. On the one hand, the spectrum is restricted by the aperture of fibres, so we can only trace a part of the galaxy (especially larger or nearer one) through the spectrum. Moreover, when we probe the emission lines radiated from H II regions, which tend to have higher dust density, we probably get a higher extinction. On the other hand, the companion component and the stellar population interfere with the measurement of integrated flux. It is difficult to decompose the members and deduct the contributions of continuum as well as stellar population simultaneously. So a Gaussian function plus a quadratic polynomial fitting are applied to the emission lines of observed spectra in our measurement. It may also lead to an overestimation of the values. Moreover, color magnitude measurement may also

be affected by intergalactic medium and other members in its cluster (if so). To illustrate this result and explore the intrinsic dust distribution, the high-resolution images and the IFU spectra are needed.

The difference between two extinction values ($\Delta E(B - V) = E(B - V)_{bg} - E(B - V)_{fg}$) can reflect dust features of the traced regions of the foreground galaxy in a clean environment. However, for most overlapping galaxy pairs, there are many objects around them, which will bias the estimation. Especially, the bias will be more severe for the galaxy pairs with larger distances.

4 CONCLUSIONS AND DISCUSSIONS

The main works. An automatic search method of SGPs based on the fuzzy recognition is presented in this paper. The basic idea is to detect and identify the galaxy spectra which have two sets of emission lines from SDSS DR9. Limited by some factors such as low S/N, various broadening and other pre-processing errors, a lot of emission lines can not be identified accurately. Therefore, a membership degree is defined to measure the confidence of these lines. A SGPs sample of 165 targets is mined out by different thresholds and visual inspection. In this sample mined out by the above method, the minimum and maximum Δz is 0.0055 and 0.27 respectively, which indicates that there are nearly no interacting pairs. All spectra in our sample are divided into four grades (A, B, C, D) according to the membership degrees and those spectra graded ‘A’ are used for a estimation of the

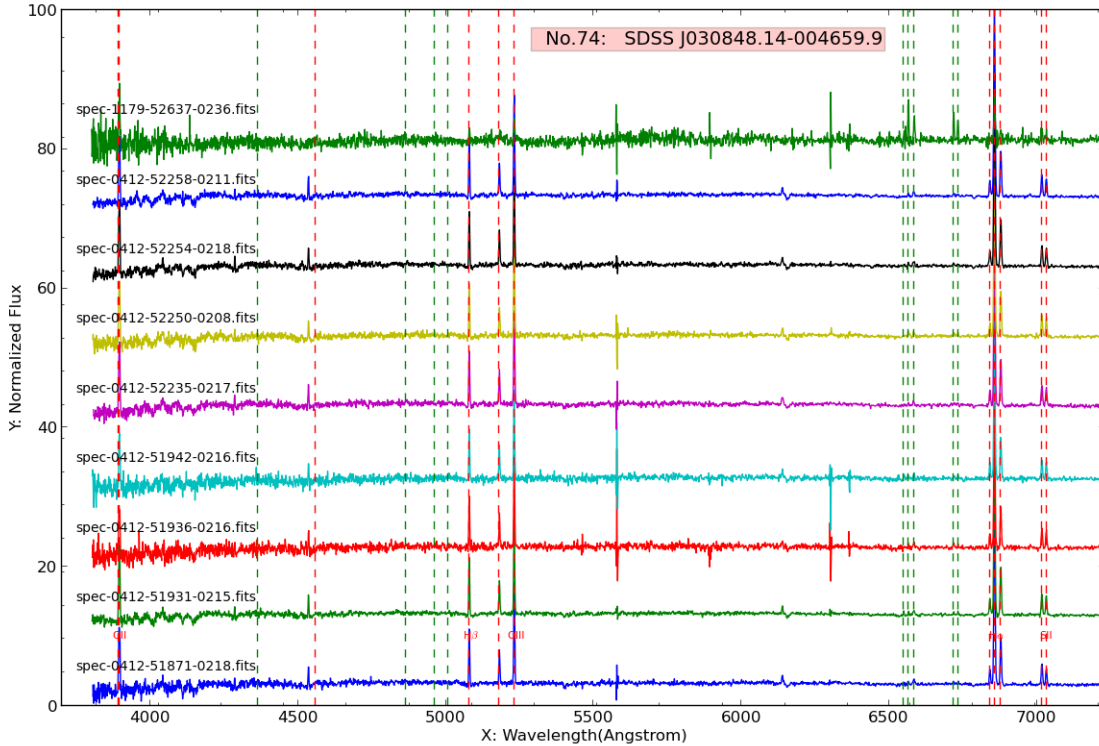


Figure 4. The spectra of ‘SDSS J030848.14-004659.9’ with nine observations sorted by modified Julian date (MJD). All spectra are scaled and shifted in one coordinate system. The fits names are marked on the top left of each spectrum. The common emission lines of two redshift systems are marked with green and red dashed lines, respectively.

dust extinction. Additionally, analyses for a series of observations of one SGP from 165 systems indicate that a newly star-forming region of our Milky Way might occur.

By aid of the visual inspection of spectra and the contour lines from images, it is easy to get the relative position between these objects. In this paper, all images of our sample are classified into eight subclasses. Some images may be misclassified due to the limitation of observational capabilities and the complexity of environments around the targets. The four subclasses, with a single image component, are interesting since the foreground system may be a dwarf galaxy lost in the background light.

About the method. The method presented in this paper is useful to measure the confidence of SGPs. The membership degree defined in previous text plays a key role in the searching process. Using high thresholds of the membership degree will lead to the strong confidence of SGPs and a high probability of missing some SGPs with low spectral quality. On the contrary, the missed SGPs can be recovered when using low thresholds of the membership degree, and yet pseudo SGPs may be mixed into the result sample in such condition. Accordingly, the reasonable choice of membership degree thresholds is vitally important in searching process. Anyway, the searching result is reliable after trying different thresholds repeatedly.

On the other hand, there may still be some missing spectra in the searching process since the approach highly depends on the fitting quality of lines by Gaussian function. Poor fittings in some cases may be caused by weakness or

deformation of the lines. In addition, this method has limitations in detecting the absorption features because some blended absorption lines could not be fitted by a single Gaussian function and the molecular bands could not be represented by Gaussian. Therefore, our method has only succeed in searching for dual-emission systems in single galaxy spectrum so far. Improving the measurement ability of the membership degree for uncertainty nature will be very valuable for those cases mentioned above.

In the end, we hope that this paper can be a clue for follow-up observational study. First of all, the further identification observations for overlapping galaxies pairs are needed. Then, Limited by the fibre aperture, only 3” region of some targets can be traced. Thus, larger aperture telescope or IFU techniques are valuable for the studying of dust distribution. Additionally, higher resolution photometric images are also helpful to analyze environments of these targets.

ACKNOWLEDGEMENTS

This work is supported by National Key Basic Research Program of China (Grant No. 2014CB845700), and the National Natural Science Foundation of China (Grant Nos 11233004, 61272263, 61301245).

The authors would like to thank the referee from Professor Keel, William for the many suggestions that have helped improve the manuscript, Professor Sijiong Zhang for helpful suggestions, and Mr Jie Zheng, Miss Shuo Zhang, Miss

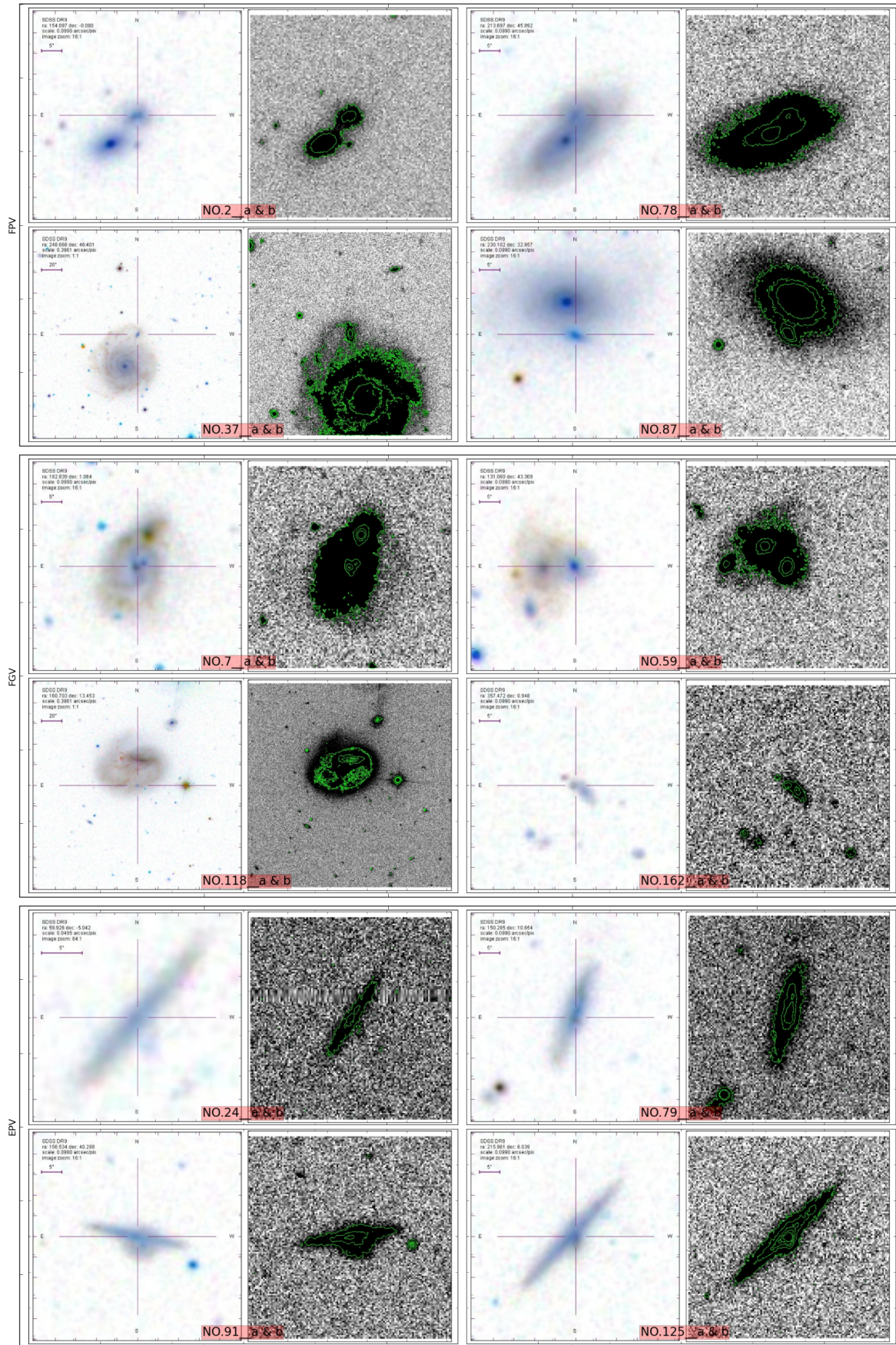


Figure 5. The examples of three subclasses (FPV, FGV, EPV) with multiple image components. The serial numbers are shown in the bottom center of every image. The scale of images is indicated in the top left corner. The orientation is north up and east left. For every image, the left panel is a multicolour image and the right one is the corresponding contour map representation in the SDSS r-band image.

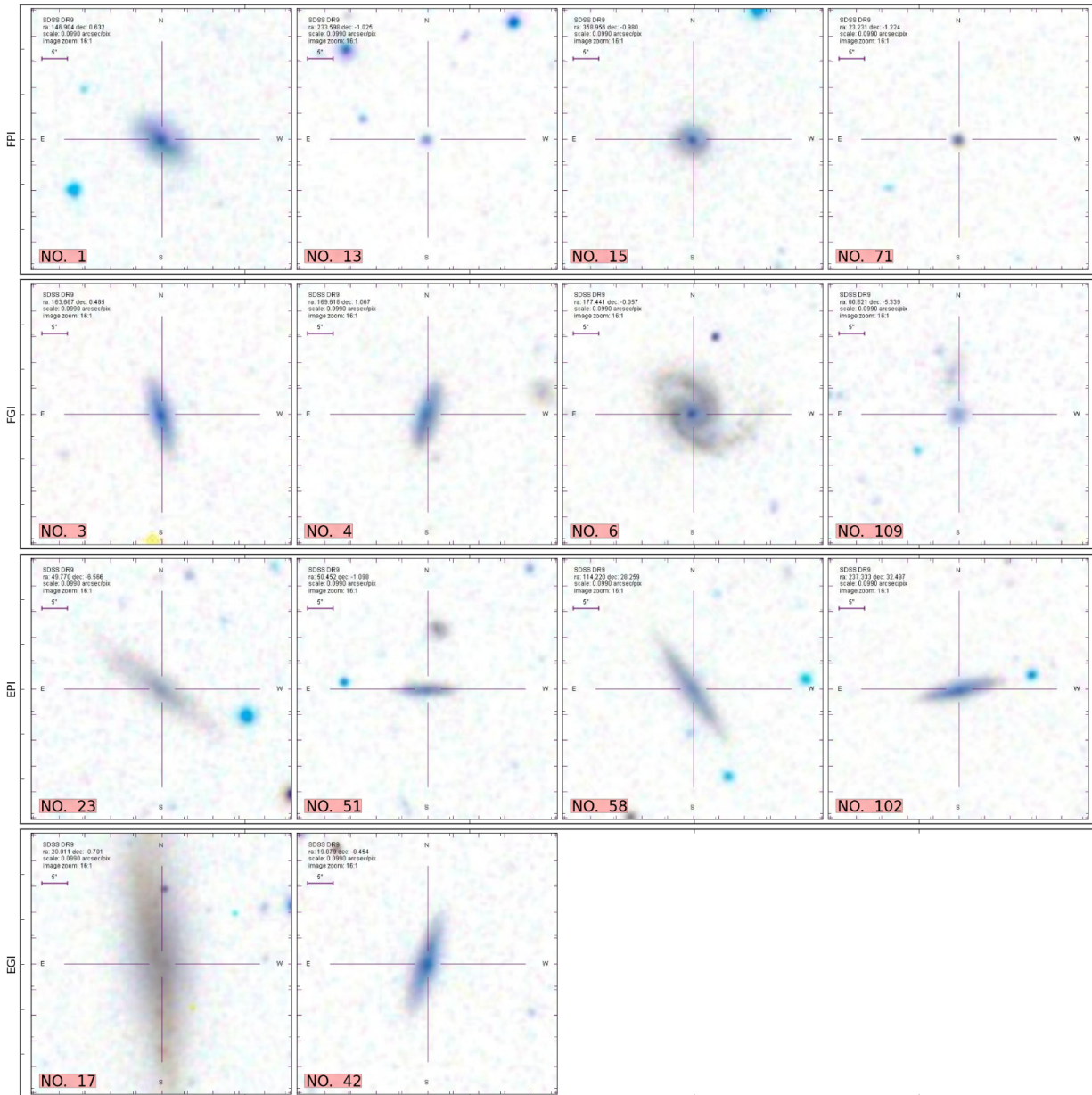


Figure 6. The examples of four subclasses (FPI, FGI, EPI, EGI) with single image component. Except that the contour map representations are absent, all symbols are the same as Figure 5.

Yanxin Guo, Miss Yu Bai for enthusiastic help and useful initial data organization and reduction.

Funding for SDSS-III has been provided by the Alfred P. Sloan Foundation, the Participating Institutions, the National Science Foundation, and the U.S. Department of Energy Office of Science. The SDSS-III web site is <http://www.sdss3.org/>.

SDSS-III is managed by the Astrophysical Research Consortium for the Participating Institutions of the SDSS-III Collaboration including the University of Arizona, the Brazilian Participation Group, Brookhaven National Laboratory, University of Cambridge, Carnegie Mellon University, University of Florida, the French Participation Group, the German Participation Group, Harvard University, the Instituto de Astrofísica de Canarias, the Michigan

State/Notre Dame/JINA Participation Group, Johns Hopkins University, Lawrence Berkeley National Laboratory, Max Planck Institute for Astrophysics, Max Planck Institute for Extraterrestrial Physics, New Mexico State University, New York University, Ohio State University, Pennsylvania State University, University of Portsmouth, Princeton University, the Spanish Participation Group, University of Tokyo, University of Utah, Vanderbilt University, University of Virginia, University of Washington, and Yale University.

REFERENCES

Ahn C. P., Alexandroff R., Prieto C. A., Anderson S. F., Anderton T., Andrews B. H., Aubourg É., Bailey S., Balbinot E., Barnes R., et al., 2012, *ApJS*, 203, 21

Table 4. Dust Properties for 44 Grade ‘A’ SGPs

No.	Foreground Galaxy		Background Galaxy	
	$H\alpha/H\beta$	E (B-V)	$H\alpha/H\beta$	E (B-V)
2	6.08±0.46	0.67±0.01	4.34±0.62	0.38±0.02
12	4.58±0.26	0.42±0.01	5.33±1.47	0.56±0.04
16	4.55±0.23	0.41±0.01	11.43±5.36	1.32±0.07
27	3.26±0.58	0.11±0.03	10.78±6.41	1.25±0.09
29	4.17±0.86	0.33±0.03	4.04±0.90	0.31±0.03
30	4.36±0.62	0.37±0.02	4.25±0.25	0.35±0.01
41	3.88±1.00	0.27±0.04	4.60±0.54	0.42±0.02
43	3.14±0.07	0.08±0.00	4.44±0.52	0.41±0.02
45	3.43±0.65	0.16±0.03	4.30±1.01	0.37±0.04
47	4.29±1.62	0.35±0.06	5.50±2.13	0.61±0.06
50	3.48±1.77	0.17±0.08	3.16±2.42	0.09±0.12
51	2.82±1.03	-0.01±0.06	4.81±1.13	0.45±0.04
52	3.50±0.33	0.17±0.01	4.66±0.39	0.42±0.01
53	2.98±1.51	0.03±0.08	5.09±0.88	0.53±0.03
55	10.51±1.35	1.15±0.02	3.82±1.88	0.26±0.08
63	3.99±0.58	0.29±0.02	3.26±0.24	0.12±0.01
70	3.74±0.26	0.23±0.01	5.78±0.53	0.63±0.01
73	2.71±0.41	-0.05±0.02	2.12±2.81	-0.27±0.20
76	4.24±1.46	0.37±0.05	7.37±7.45	0.88±0.15
83	4.84±1.13	0.47±0.04	1.94±1.26	-0.36±0.10
94	3.47±0.32	0.17±0.01	3.05±0.49	0.06±0.02
95	3.48±0.39	0.17±0.02	7.82±2.87	0.94±0.06
103	4.32±0.59	0.36±0.02	2.11±0.13	-0.26±0.01
113	10.55±5.79	1.12±0.08	4.56±2.07	0.41±0.07
114	5.17±2.05	0.53±0.06	4.92±1.51	0.49±0.05
115	5.00±1.01	0.49±0.03	3.98±0.30	0.30±0.01
121	4.37±0.77	0.37±0.03	5.66±0.94	0.60±0.03
123	3.98±0.76	0.28±0.03	6.67±7.60	0.77±0.17
124	10.08±2.87	1.09±0.04	6.44±3.01	0.71±0.07
129	2.48±0.21	-0.12±0.01	3.48±1.61	0.17±0.07
131	3.86±0.28	0.26±0.01	2.08±0.24	-0.28±0.02
132	2.94±0.63	0.02±0.03	3.32±2.08	0.13±0.10
135	4.19±1.77	0.33±0.06	2.76±2.40	-0.04±0.13
136	3.82±0.14	0.26±0.01	3.05±0.17	0.06±0.01
138	3.28±0.39	0.12±0.02	4.35±1.58	0.39±0.06
139	3.66±0.80	0.21±0.03	6.81±0.56	0.78±0.01
141	3.13±0.32	0.08±0.02	9.70±2.19	1.13±0.03
146	3.01±0.38	0.04±0.02	6.22±1.47	0.69±0.04
150	3.46±0.32	0.16±0.01	5.35±3.15	0.56±0.09
152	3.97±0.16	0.28±0.01	4.21±1.96	0.35±0.07
154	5.84±4.86	0.63±0.13	14.41±7.61	1.45±0.08
158	3.09±0.28	0.07±0.01	4.74±1.25	0.44±0.04
160	5.92±1.34	0.65±0.03	4.08±0.43	0.34±0.02
161	4.57±0.57	0.43±0.02	3.34±0.67	0.15±0.03

NOTES:

1. The ratios of $H\alpha$ and $H\beta$ are integrated-flux-ratios after fitted by Gaussian function and a quadratic polynomial. E (B-V) are estimated by equation 5 and the unit is Mag.
2. The corresponding errors are derived from the errors of integrated flux measurement according to the law of error propagation.

Allam S. S., Tucker D. L., Smith J. A., Lee B. C., Annis J., Lin H., Karachentsev I. D., Laubscher B. E., 2004, *AJ*, 127, 1883

Berlind A. A., Frieman J., Weinberg D. H., Blanton M. R., Warren M. S., Collaboration S., 2006, *ApJS*, 167, 1

Blanton M. R., Berlind A. A., 2007, *AJ*, 664, 791

Calzetti D., Armus L., Bohlin R. C., Kinney A. L., Koornneef J., Storchi-Bergmann T., 2000, *AJ*, 533, 682

Chen X. Y., Liang Y. C., Hammer F., Zhao Y. H., Zhong G. H., 2009, *A&A*, 495, 457

Domingue D. L., Keel W. C., Ryder S. D., White III R. E., 1999, *AJ*, 118, 1542

Domingue D. L., Keel W. C., White III R. E., 2000, *AJ*, 545, 171

Dressler Alan 1980, *ApJ*, 236, 351

Eke V. R., Baugh C. M., Cole S., Frenk C. S., Norberg P., Peacock J. A., Baldry I. K., Bland-Hawthorn J., Bridges T., Cannon R., Colless M., Collins C., Couch W., 2004, *MNRAS*, 348, 866

Ellison S. L., Mendel J. T., Scudder J. M., Patton D. R., 2013a, *MNRAS*, 430, 3128

Ellison S. L., Mendel J. T., Scudder J. M., Patton D. R., 2013b, *MNRAS*, 435, 3627

Ellison S. L., Patton D. R., Mendel J. T., Scudder J. M., 2011, *MNRAS*, 418, 2043

Ellison S. L., Patton D. R., Simard L., McConnachie A. W., 2008, *AJ*, 135, 1877

Ellison S. L., Patton D. R., Simard L., McConnachie A. W., Baldry I. K., Mendel J. T., 2010, *MNRAS*, 407, 1514

Ge J.-Q., Hu C., Wang J.-M., Bai J.-M., Zhang S., 2012, *ApJS*, 201, 31

Holwerda B., Keel W., Bolton A., 2007a, *AJ*, 134, 2385

Holwerda B. W., Keel W. C., 2013, *A&A*, 556, A42

Holwerda B. W., Keel W. C., Bolton A., 2007b, *AJ*, 134, 2385

Hou A., Parker L. C., Balogh M. L., McGee S. L., Wilman D. J., Connelly J. L., Harris W. E., Mok A., Mulchaey J. S., Bower R. G., et al., 2013, *MNRAS*, 435, 1715

Kauffmann G., Heckman T. M., Tremonti C., Brinchmann J., Charlot S., White S. D., Ridgway S. E., Brinkmann J., Fukugita M., Hall P. B., et al., 2003, *MNRAS*, 346, 1055

Keel W. C., Manning A. M., Holwerda B. W., Mezzoprete M., Lintott C. J., Schawinski K., Gay P., Masters K. L., 2013, *PASP*, 125, 2

Keel W. C., White III R. E., 2001, *AJ*, 121, 1442

Kennicutt J., Robert C., 1992, *ApJ*, 388, 310

Kewley L. J., Dopita M., Sutherland R., Heisler C., Trevena J., 2001, *AJ*, 556, 121

Kopparapu R. K., Hanna C., Kalogera V., O’Shaughnessy R., González G., Brady P. R., Fairhurst S., 2008, *ApJ*, 675, 1459

Krabbe A., Rosa D., Dors O., Pastoriza M., Winge C., Hägele G., Cardaci M., Rodrigues I., 2014, *MNRAS*, 437, 1155

Lewis I., Balogh M., De Propriis R., Couch W., Bower R., Offer A., Bland-Hawthorn J., Baldry I. K., Baugh C., Bridges T., et al., 2002, *MNRAS*, 334, 673

Liu X., Shen Y., Strauss M. A., Hao L., 2011, *ApJ*, 737, 101

McConnachie A. W., Patton D. R., Ellison S. L., Simard L., 2009, *MNRAS*, 395, 255

Marino A., Plana H., Rampazzo R., Bianchi L., Rosado M., Bettoni D., Galletta G., Mazzei P., Buson L., Ambrocio-Cruz P., Gabbasov R. F., 2013, *MNRAS*, 428, 476

Merchán M. E., Zandivarez A., 2005, *ApJ*, 630, 759

Nikolic B., Cullen H., Alexander P., 2004, *MNRAS*, 355, 874

Patton D. R., Ellison S. L., Simard L., McConnachie A. W., Mendel J. T., 2011, *MNRAS*, 412, 591

Patton D. R., Torrey P., Ellison S. L., Mendel J. T., Scud-

- der J. M., 2013, MNRAS, 433, L59
Satyapal S., Ellison S. L., McAlpine W., Hickox R. C., Patton D. R., Mendel J. T., 2014, MNRAS, 441, 1297
Scudder J. M., Ellison S. L., Torrey P., Patton D. R., Mendel J. T., 2012, MNRAS, 426, 549
Tsalmantza P., Hogg D. W., 2012, ApJ, 753, 122
Tyler K., Rieke G., Bai L., 2013, AJ, 773, 86
Wake D. A., Collins C. A., Nichol R. C., Jones L. R., Burke D. J., 2005, AJ, 627, 186
White R. E., Keel W. C., 1992, Nature, 359, 129
Wilman D., Pierini D., Tyler K., McGee S., Oemler Jr A., Morris S., Balogh M., Bower R., Mulchaey J., 2008, AJ, 680, 1009
Zadeh L. A., 1965, Information and control, 8, 338
Zhang J., Zhang S., Chang K. H., Qin X., 2014, International Journal of Systems Science, 45, 1170
Zhang J., Zhao X., Zhang S., Yin S., Qin X., 2013, Knowledge-Based Systems, 41, 77

APPENDIX : SAMPLE LIST

Table 1: SGP_s sample selected from SDSS DR9

No.	Object Name	RA	DEC	z1	z2	Level	Environment	Note
1	SDSS J094736.91+003755.8	146.90380	0.63221	0.0628±0.00001	0.1756±0.00341	C	FPI	
2*	SDSS J101623.29-000449.6	154.09699	-0.08044	0.0948±0.00000	0.1406±0.00001	A	FPV	
3	SDSS J105444.99+002904.7	163.68746	0.48461	0.1051±0.01508	0.1257±0.00005	B	FGI	1
4	SDSS J111828.31+010400.1	169.61797	1.06670	0.0636±0.00000	0.1776±0.01508	C	FGI	1, 2, 3
5	SDSS J111500.42-005116.0	168.75176	-0.85442	0.1003±0.00003	0.2711±0.01508	C	FGV	1
6	SDSS J114945.82-000325.3	177.44094	-0.05702	0.0952±0.00001	0.1967±0.00097	C	FGI	1
7*	SDSS J121121.35+010348.9	182.83896	1.06361	0.0470±0.00000	0.1248±0.00003	B	FGV	1, 4
8	SDSS J130405.75-003508.8	196.02395	-0.58576	0.0468±0.00001	0.1465±0.01508	D	FGI	1
9	SDSS J133408.42+002840.2	203.53509	0.47788	0.0767±0.00008	0.1590±0.01508	C	FGV	1
10	SDSS J140157.15-011108.8	210.48812	-1.18586	0.0255±0.00003	0.2711±0.01508	C	FGV	1, 2
11*	SDSS J141546.22-011112.4	213.94254	-1.18681	0.0499±0.00000	0.1494±0.01508	B	FGV	1, 2
12*	SDSS J160818.74-002745.4	242.07809	-0.46262	0.1128±0.01508	0.1237±0.00000	A	FPI	
13	SDSS J153423.52-010130.3	233.59799	-1.02508	0.1031±0.00021	0.3737±0.10000	D	FPI	
14*	SDSS J233129.22+005217.1	352.87180	0.87145	0.1392±0.00003	0.3157±0.00005	B	FPV	
15	SDSS J235549.52-005847.7	358.95639	-0.97992	0.0748±0.00000	0.1765±0.01508	C	FPI	
16*	SDSS J010304.26+002827.3	15.76774	0.47427	0.0670±0.00000	0.2570±0.00003	A	FPI	
17*	SDSS J012314.54-004204.5	20.81058	-0.70130	0.0066±0.01508	0.1987±0.00015	C	EGI	
18	SDSS J013444.28+152421.9	23.68449	15.40609	0.0342±0.00001	0.1755±0.00662	B	FPI	
19	SDSS J073926.08+392713.9	114.85872	39.45386	0.0615±0.00002	0.2173±0.01508	B	FPI	
20	SDSS J085652.80+545749.4	134.22004	54.96374	0.0382±0.00000	0.2711±0.01508	D	FGI	2
21*	SDSS J092833.76+580628.8	142.14068	58.10804	0.1000±0.01508	0.1055±0.01508	C	FPI	
22*	SDSS J031750.07-061134.7	49.45862	-6.19297	0.0000±0.01508	0.1708±0.00163	B	FPI	
23	SDSS J031904.90-063357.6	49.77042	-6.56604	0.0000±0.00001	0.0412±0.00002	B	EPI	
24	SDSS J035942.19-050232.3	59.92583	-5.04231	0.0001±0.00000	0.0652±0.00000	B	EPV	
25	SDSS J040708.86-054455.1	61.78695	-5.74864	0.0001±0.01508	0.1088±0.00001	B	FPI	
26	SDSS J124225.05+664807.2	190.60441	66.80203	0.0618±0.00002	0.1745±0.01508	C	FPI	
27*	SDSS J115353.75+011914.5	178.47396	1.32068	0.0784±0.01508	0.2305±0.00067	A	FGV	1
28	SDSS J120600.06+023522.9	181.50028	2.58972	0.0683±0.01508	0.1581±0.00001	D	EPI	
29	SDSS J131105.31+022528.3	197.77220	2.42456	0.0675±0.00000	0.1187±0.01508	A	FGI	2
30*	SDSS J131105.31+022528.3	197.77220	2.42456	0.0675±0.01508	0.1186±0.01508	A	FGI	2
31*	SDSS J132120.68+032905.9	200.33617	3.48500	0.0823±0.00000	0.2704±0.00022	B	FGI	2
32	SDSS J100733.49+574934.3	151.88959	57.82624	0.1874±0.00003	0.2714±0.00010	C	FPI	
33	SDSS J090202.57+033525.5	135.51072	3.59044	0.0258±0.00000	0.2714±0.01508	D	FGI	2
34	SDSS J141133.07+042854.1	212.88785	4.48168	0.0185±0.00000	0.2185±0.01508	B	FGV	
35	SDSS J145247.81+044847.7	223.19921	4.81324	0.0645±0.00001	0.1771±0.01508	C	FGI	2
36*	SDSS J150630.83+043100.0	226.62850	4.51666	0.0353±0.00000	0.0723±0.00003	B	FPI	
37*	SDSS J163440.40+462402.4	248.66836	46.40070	0.0184±0.00004	0.1405±0.01508	C	FPV	
38	SDSS J213706.38-065950.0	324.27660	-6.99722	0.0604±0.00001	0.1765±0.01508	C	FPI	
39*	SDSS J233505.81-101625.2	353.77426	-10.27369	0.0595±0.00000	0.2106±0.00002	B	FPV	
40	SDSS J003345.57-093044.1	8.43987	-9.51226	0.0893±0.00001	0.1628±0.01508	B	FPI	
41*	SDSS J003959.54-084454.5	9.99815	-8.74849	0.0942±0.00001	0.1178±0.00001	A	FPV	2
42	SDSS J011930.92-082716.1	19.87889	-8.45447	0.0750±0.00003	0.1753±0.01508	D	EGI	2
43*	SDSS J004717.77-002233.4	11.82407	-0.37584	0.1210±0.00000	0.2062±0.00003	A	FPV	
44	SDSS J005424.39+011027.5	13.60168	1.17433	0.0861±0.00001	0.1806±0.01508	B	FPI	
45*	SDSS J014742.29-010806.8	26.92625	-1.13524	0.0438±0.00000	0.1346±0.00001	A	FPI	
46	SDSS J023558.17+011529.0	38.99244	1.25810	0.0683±0.00000	0.1236±0.00012	D	FPV	4,5
47*	SDSS J214425.44+114423.0	326.10600	11.73974	0.0259±0.00001	0.2184±0.00005	A	FGV	2
48	SDSS J233150.43+132827.9	352.96013	13.47441	0.1372±0.00003	0.2714±0.01508	C	EPI	
49*	SDSS J081117.05+380000.0	122.82103	38.00000	0.1022±0.00000	0.1834±0.00004	B	FPV	
50	SDSS J031201.75+005611.8	48.00735	0.93659	0.0699±0.01508	0.2229±0.01508	A	FPI	
51	SDSS J032148.43-010552.7	50.45185	-1.09802	0.0000±0.00001	0.0673±0.00000	A	EPI	
52*	SDSS J032043.66-001753.9	50.18198	-0.29845	0.0001±0.00001	0.0380±0.00001	A	EPI	
53*	SDSS J030423.66-005823.7	46.09863	-0.97329	0.0309±0.00002	0.1915±0.01508	A	FPV	
54*	SDSS J163627.02+384021.5	249.11260	38.67265	0.0353±0.00003	0.2707±0.01508	C	EPI	
55*	SDSS J085805.75+410324.1	134.52398	41.05673	0.0883±0.00002	0.1403±0.00002	A	FGV	2

Continued on next page

Table 1: – continued from previous page

No.	Object Name	RA	DEC	z1	z2	Grade	Environment	Note
56	SDSS J090954.91+423944.4	137.47878	42.66233	0.0412±0.00001	0.2705±0.01508	C	FPI	
57*	SDSS J113618.85+043455.9	174.07859	4.58222	0.0918±0.00002	0.2900±0.00013	D	FPI	
58	SDSS J073652.76+281534.1	114.21989	28.25949	0.0603±0.00001	0.2710±0.01508	B	EPI	
59	SDSS J084414.50+431830.6	131.06047	43.30852	0.0274±0.00004	0.1059±0.00008	B	FGV	6
60	SDSS J100707.60+534604.7	151.78168	53.76803	0.0450±0.00000	0.1877±0.01508	D	FGI	2
61*	SDSS J101040.39+540642.1	152.66831	54.11170	0.0472±0.00003	0.2312±0.00002	B	FPV	2
62	SDSS J103828.47+560244.0	159.61869	56.04558	0.0464±0.00001	0.0917±0.00005	B	FPI	
63*	SDSS J141546.22-011112.4	213.94259	-1.18682	0.0499±0.00000	0.1493±0.00000	A	FPV	1, 2
64*	SDSS J132728.33+573904.8	201.86813	57.65136	0.0774±0.00000	0.1155±0.00004	B	FPI	
65	SDSS J113541.07+484813.2	173.92113	48.80368	0.0367±0.00002	0.1580±0.00010	D	FGV	2
66*	SDSS J170254.76+341035.3	255.72818	34.17649	0.0364±0.00001	0.0969±0.00000	C	FGV	2
67*	SDSS J210607.89-004756.6	316.53288	-0.79904	0.0347±0.00000	0.1146±0.00000	B	FPI	
68*	SDSS J223541.83-002948.6	338.92432	-0.49684	0.0587±0.00003	0.2149±0.00013	B	FPV	
69	SDSS J074619.61+275512.9	116.58173	27.92025	0.0757±0.00000	0.3170±0.01508	C	FPI	
70*	SDSS J025450.49+010315.6	43.71036	1.05441	0.0437±0.00000	0.1365±0.01508	A	FGV	
71	SDSS J013255.51-011325.7	23.23134	-1.22384	0.1601±0.00002	0.2841±0.01000	D	FPI	
72*	SDSS J004647.31-004214.5	11.69716	-0.70403	0.0161±0.00001	0.1867±0.00009	D	FGV	
73	SDSS J033655.06-001549.0	54.22944	-0.26362	0.0000±0.01508	0.1486±0.01508	A	FPI	
74	SDSS J030848.14-004659.9	47.20060	-0.78332	0.0001±0.00003	0.0445±0.00014	B	FPI	
75*	SDSS J090601.23+365851.4	136.50514	36.98097	0.1070±0.00006	0.2637±0.00017	D	FPI	
76*	SDSS J091636.13+364214.2	139.15056	36.70395	0.2034±0.00005	0.2110±0.01508	A	FPI	
77	SDSS J054956.59-002613.2	87.48583	-0.43703	0.0000±0.01508	0.1076±0.00000	B	EPI	
78*	SDSS J141447.34+455331.6	213.69730	45.89212	0.0406±0.00001	0.0996±0.00001	B	FPV	
79*	SDSS J100108.40+103914.3	150.28504	10.65399	0.0888±0.00000	0.1071±0.00006	B	EPV	
80*	SDSS J141109.08+545652.4	212.78781	54.94788	0.0422±0.01508	0.0764±0.00000	B	FPV	2, 5
81*	SDSS J145123.60+512833.9	222.84835	51.47610	0.0353±0.00000	0.1548±0.00001	B	FPI	
82	SDSS J153353.20+450929.6	233.47166	45.15823	0.0769±0.00000	0.2062±0.01508	D	EPI	2
83	SDSS J155019.92+445310.0	237.58306	44.88611	0.1437±0.00003	0.1986±0.00036	A	FPI	
84*	SDSS J164043.33+295611.6	250.18052	29.93657	0.0461±0.00001	0.1563±0.00002	B	FPV	
85*	SDSS J115018.78+452911.8	177.57832	45.48662	0.0108±0.01508	0.1403±0.00001	B	FPV	
86	SDSS J130847.08+444300.7	197.19618	44.71688	0.0718±0.00001	0.1148±0.00006	B	FPI	
87*	SDSS J152024.36+325126.4	230.10153	32.85735	0.0619±0.00001	0.0797±0.00034	B	FPV	7
88*	SDSS J144951.22+410721.9	222.46341	41.12276	0.0275±0.00002	0.1708±0.00006	B	FPI	
89*	SDSS J145921.13+384645.8	224.83806	38.77941	0.0918±0.00001	0.1853±0.00000	B	FPV	8
90*	SDSS J161754.02+320627.4	244.47515	32.10763	0.0630±0.00000	0.1174±0.00031	B	FPV	5
91*	SDSS J102608.19+401752.7	156.53415	40.29800	0.0642±0.00001	0.1277±0.00001	B	EPV	
92*	SDSS J004518.45+002546.6	11.32692	0.42967	0.0840±0.00000	0.1241±0.01508	C	FPI	
93	SDSS J010047.37-001136.8	15.19744	-0.19363	0.1215±0.00001	0.2212±0.01508	D	EPI	
94*	SDSS J012437.25-000911.2	21.15523	-0.15309	0.0926±0.00000	0.1372±0.00001	A	FPI	
95*	SDSS J011759.09-000206.2	19.49619	-0.03507	0.1054±0.01508	0.2078±0.00023	A	FPI	
96*	SDSS J011701.92-010733.1	19.25809	-1.12588	0.1143±0.01156	0.1243±0.00014	C	FPI	
97*	SDSS J234850.00-010005.3	357.20837	-1.00149	0.2128±0.00004	0.3418±0.01508	D	FPI	
98*	SDSS J003148.12+001132.3	7.95055	0.19233	0.0949±0.01508	0.1254±0.00000	B	FPI	
99*	SDSS J031955.18-001349.7	49.97998	-0.23052	0.0001±0.01508	0.1313±0.00007	B	FGI	9
100*	SDSS J165013.06+204431.2	252.55445	20.74200	0.0816±0.00000	0.1817±0.00002	B	FPV	
101*	SDSS J163500.59+244720.9	248.75246	24.78917	0.0577±0.00000	0.1529±0.00002	B	FPV	
102	SDSS J154919.85+322950.9	237.33272	32.49748	0.0556±0.00000	0.2049±0.01508	C	EPI	
103*	SDSS J093356.59+344108.6	143.48583	34.68575	0.0427±0.01508	0.0607±0.00000	A	FGI	3
104*	SDSS J105831.73+115647.0	164.63228	11.94640	0.0887±0.01508	0.1305±0.00002	C	FPV	
105*	SDSS J111624.10+110611.5	169.10045	11.10320	0.0199±0.00000	0.0650±0.00001	B	FPI	10
106	SDSS J113638.25+125125.2	174.15939	12.85702	0.1179±0.01508	0.1560±0.00067	B	FPI	
107*	SDSS J113319.23+073027.9	173.33014	7.50778	0.1351±0.00001	0.1584±0.00015	B	FPV	
108	SDSS J040008.56-063023.4	60.03570	-6.50651	0.0001±0.00006	0.2392±0.00003	C	FPI	
109	SDSS J040317.11-052020.1	60.82131	-5.33893	0.0001±0.00003	0.2166±0.00002	B	FGI	9
110	SDSS J040705.67-060616.3	61.77365	-6.10455	0.0001±0.00003	0.2728±0.00009	C	FPI	
111*	SDSS J040804.87-061635.6	62.02031	-6.27657	0.0001±0.00000	0.2278±0.00001	D	FPI	
112*	SDSS J152411.38+291220.4	231.04742	29.20569	0.1131±0.01508	0.1512±0.00002	C	FPI	

Continued on next page

Table 1: – continued from previous page

No.	Object Name	RA	DEC	z1	z2	Grade	Environment	Note
113*	SDSS J124315.93+131438.7	190.81641	13.24409	0.0029±0.00007	0.0674±0.00000	A	FGV	
114*	SDSS J135420.79+104540.8	208.58665	10.76135	0.1229±0.00001	0.1386±0.01508	A	FPI	
115*	SDSS J145237.94+091835.3	223.15813	9.30983	0.0547±0.00001	0.1627±0.00003	A	FPV	
116*	SDSS J150645.77+095133.0	226.69072	9.85917	0.0853±0.01508	0.2094±0.00002	C	FPI	
117	SDSS J151241.12+083929.5	228.17137	8.65820	0.0783±0.00004	0.1584±0.00009	D	FPI	
118*	SDSS J104248.72+132710.8	160.70303	13.45300	0.0041±0.00001	0.2025±0.00003	B	FGV	11
119*	SDSS J104456.19+135040.3	161.23418	13.84454	0.0376±0.00001	0.0930±0.00003	B	FPV	
120*	SDSS J110335.37+141329.1	165.89738	14.22476	0.0462±0.00001	0.2645±0.01508	B	FPI	
121*	SDSS J112810.02+144124.9	172.04178	14.69026	0.0378±0.00001	0.0791±0.00000	A	FPI	5
122*	SDSS J085433.57+085243.1	133.63991	8.87866	0.0001±0.00000	0.0630±0.00001	C	FPI	
123	SDSS J085357.03+085401.1	133.48768	8.90032	0.0002±0.00001	0.1708±0.00008	A	FPV	9
124*	SDSS J151147.25+055552.2	227.94689	5.93117	0.0528±0.00000	0.0791±0.00002	A	FPI	
125*	SDSS J142350.68+060219.0	215.96120	6.03861	0.0358±0.01508	0.0557±0.01508	B	EPV	
126	SDSS J144928.24+063743.5	222.36770	6.62877	0.0999±0.00000	0.1753±0.01508	B	FPI	
127*	SDSS J162757.34+201030.0	246.98894	20.17503	0.0365±0.00001	0.1516±0.00003	D	EPI	
128	SDSS J072626.89+440844.1	111.61207	44.14561	0.0542±0.01508	0.1752±0.01508	D	EPI	
129	SDSS J075741.90+532435.2	119.42459	53.40979	0.0002±0.00000	0.0429±0.00001	A	FPI	
130*	'1879-54478-0420'	None	None	0.0001±0.00001	0.2048±0.00007	B	Non	
131*	SDSS J101749.04+360004.2	154.45438	36.00118	0.0545±0.00000	0.0896±0.00002	A	FPI	
132*	SDSS J103029.76+304621.3	157.62404	30.77260	0.0441±0.00000	0.1376±0.00003	A	FPI	
133	SDSS J111255.81+391644.1	168.23258	39.27892	0.0963±0.00000	0.1563±0.00006	B	FPI	
134	SDSS J124858.58+365308.8	192.24413	36.88578	0.1517±0.00000	0.1986±0.01508	C	FPI	
135*	SDSS J134741.29+382535.8	206.92208	38.42662	0.0091±0.00000	0.2127±0.00037	A	FGV	
136*	SDSS J105644.24+321959.9	164.18436	32.33333	0.1282±0.00000	0.1402±0.00001	A	FPV	
137*	SDSS J075452.04+155546.4	118.71685	15.92959	0.1025±0.00004	0.1109±0.00002	B	FPI	
138*	SDSS J120331.40+334112.8	180.88085	33.68691	0.0355±0.00001	0.1780±0.00001	A	FPV	
139*	SDSS J134951.29+281032.0	207.46375	28.17557	0.0554±0.00000	0.1303±0.00001	A	FPV	
140*	SDSS J135112.11+262225.2	207.80049	26.37369	0.0619±0.00001	0.1416±0.00010	D	FPV	
141*	SDSS J112702.06+270850.4	171.75864	27.14735	0.0231±0.00000	0.1980±0.01508	A	FPV	5
142	SDSS J124342.12+272222.7	190.92552	27.37300	0.0245±0.00000	0.1511±0.00003	B	FPI	
143	SDSS J094830.37+265515.6	147.12649	26.92105	0.0693±0.01508	0.1033±0.00058	C	FPI	
144*	SDSS J101550.19+245406.0	153.95915	24.90168	0.0383±0.00000	0.1721±0.00030	B	FPI	
145*	SDSS J102403.67+245139.3	156.01533	24.86094	0.1063±0.00001	0.1951±0.00229	B	FGV	
146*	SDSS J095019.00+203259.1	147.57910	20.54981	0.0252±0.00000	0.1008±0.00001	A	FPV	
147	SDSS J080649.19+114202.4	121.70497	11.70067	0.0723±0.00000	0.1033±0.01508	D	FPI	
148	SDSS J085107.33+150344.0	132.78040	15.06204	0.0699±0.00001	0.2060±0.00002	B	FPV	
149*	SDSS J090434.83+132222.6	136.14515	13.37296	0.0280±0.00000	0.1861±0.00004	C	FPI	
150*	SDSS J112824.97+225422.7	172.10410	22.90631	0.0322±0.00001	0.1353±0.00011	A	FPV	
151*	SDSS J115412.76+250055.6	178.55322	25.01546	0.0738±0.01508	0.1067±0.01508	B	FPV	
152*	SDSS J162006.77+120851.1	245.02822	12.14753	0.0506±0.01508	0.1805±0.00174	A	FPV	
153*	SDSS J094914.92+132616.9	147.31218	13.43806	0.0406±0.01508	0.2945±0.00021	B	FPV	
154*	SDSS J101238.56+153334.9	153.16070	15.55971	0.0880±0.00001	0.1241±0.00005	A	FPI	
155*	SDSS J102458.65+164444.7	156.24440	16.74575	0.0452±0.00001	0.1680±0.00016	C	FPI	
156	SDSS J104132.16+171908.8	160.38401	17.31912	0.1227±0.00001	0.1755±0.00050	C	FPV	
157*	SDSS J124453.41+193913.2	191.22256	19.65369	0.0645±0.00001	0.2398±0.00002	B	FPV	
158*	SDSS J135703.93+225619.5	209.26647	22.93882	0.0123±0.01508	0.0636±0.00002	A	FPV	
159	SDSS J142249.53+214458.2	215.70640	21.74951	0.1430±0.00001	0.1914±0.01508	C	FPI	
160*	SDSS J164054.38+272845.6	250.22661	27.47936	0.1033±0.01508	0.2793±0.00002	A	FPI	
161	SDSS J024411.33-005021.0	41.04724	-0.83919	0.1806±0.00005	0.2396±0.00018	A	FPV	
162	SDSS J234953.32+005652.9	357.47218	0.94804	0.1622±0.00001	0.2148±0.00008	B	FGV	9
163	SDSS J021719.91-004555.2	34.33298	-0.76533	0.0693±0.00000	0.1497±0.00001	B	FGV	
164	SDSS J233404.08+013507.0	353.51702	1.58529	0.0440±0.00000	0.1295±0.01508	B	FPV	
165	SDSS J093830.34+381935.2	144.62642	38.32646	0.1228±0.00001	0.1808±0.00024	B	FPV	

NOTES:

1. 'No.' is the serial number for every object and it will be referred to throughout this paper. The records are marked with asterisks in the upper right corner of serial numbers if there are at least two values in XCRedshift results close to the values identified by our method.

2. The two redshifts (errors) are determined by the core wavelength of best-fit emission lines. 'Level' is classified according to

different membership degree thresholds, ‘Environment’ is classified by vision inspection and literature, and other columns are obtained from <http://www.sdss3.org/>.

3. The column ‘Note’ shows that some objects appear in the sample of literature and the values are the relevant literature number: 1. [Eke et al. \(2004\)](#), 2. [Merchán & Zandivarez \(2005\)](#), 3. [Berlind et al. \(2006\)](#), 4. [Allam et al. \(2004\)](#), 5. [Keel et al. \(2013\)](#), 6. [Holwerda et al. \(2007b\)](#), 7. [Liu et al. \(2011\)](#), 8. [Ge et al. \(2012\)](#), 9. [McConnachie et al. \(2009\)](#), 10. [Kopparapu et al. \(2008\)](#), 11. [Marino et al. \(2013\)](#).

This paper has been typeset from a \TeX / \LaTeX file prepared by the author.